Eur J Nucl Med Mol Imaging (2017) 44:598–610
DOI 10.1007/s00259-016-3521-3

ORIGINAL ARTICLE

^{18}F-fluorodeoxyglucose positron emission tomography-computed tomography in the management of adult multisystem Langerhans cell histiocytosis

Julie Obert[1,2] · Laetitia Vercellino[3] · Axel Van Der Gucht[1,3] · Constance de Margerie-Mellon[1,4] · Emmanuelle Bugnet[2] · Sylvie Chevret[1,5,6] · Gwenaël Lorillon[2] · Abdellatif Tazi[1,2,6]

Received: 26 July 2016 / Accepted: 7 September 2016 / Published online: 20 September 2016

Abstract
Purpose The standard evaluation of multisystem Langerhans cell histiocytosis (LCH) includes a clinical evaluation, laboratory tests and a skeleton/skull X-ray survey, with chest high-resolution computed tomography (HRCT) in the case of pulmonary involvement. Preliminary reports suggest that ^{18}F-fluorodeoxyglucose positron emission tomography-computed tomography (^{18}F-FDG PET-CT) may be useful for evaluating patients with LCH.
Methods Fourteen consecutive adult patients with multisystem LCH were included in this retrospective study, and were evaluated using standard procedures and ^{18}F-FDG PET-CT. The two sets of findings were compared both at baseline and during follow-up. Serial HRCT and pulmonary function tests were used to evaluate outcome in patients with lung involvement.
Results At the baseline evaluation, PET-CT identified every LCH localization found with the standard evaluation (except a mild cecum infiltration). PET-CT showed additional lesions in seven patients, mostly involving bones, and differentiated inactive from active lesions. Thyroid ^{18}F-FDG uptake was identified in three cases. No pituitary stalk ^{18}F-FDG uptake was observed in patients with pituitary LCH. Only 3/12 (25 %) patients with pulmonary LCH displayed moderate pulmonary ^{18}F-FDG uptake. During follow-up, variations (≥50 % of maximum standardized uptake) in bone ^{18}F-FDG uptake intensity were correlated with disease state and response to treatment. The absence of lung ^{18}F-FDG uptake did not preclude lung function improvement after treatment.
Conclusions Except for cases with pulmonary and pituitary involvement, ^{18}F-FDG PET-CT could replace the standard evaluation for staging of adult patients with multisystem LCH. Serial PET-CT scans are useful for evaluating treatment responses, particularly in cases with bone LCH involvement.

Keywords Langerhans cell histiocytosis · PET-CT · Management · Response to treatment

✉ Abdellatif Tazi
abdellatif.tazi@aphp.fr

[1] Université Paris Diderot, Sorbonne Paris Cité, Paris, France

[2] Centre National de Référence de l'Histiocytose Langerhansienne, Service de Pneumologie, Hôpital Saint-Louis, Assistance Publique-Hôpitaux de Paris, Paris, France

[3] Service de Médecine Nucléaire, Hôpital Saint-Louis, Assistance Publique-Hôpitaux de Paris, Paris, France

[4] Service de Radiologie, Hôpital Saint-Louis, Assistance Publique-Hôpitaux de Paris, Paris, France

[5] Service de Biostatistique et Information Médicale, Hôpital Saint-Louis, Assistance Publique-Hôpitaux de Paris, Paris, France

[6] U1153 CRESS, Biostatistics and Clinical Epidemiology Research Team, Paris, France

Introduction

Langerhans cell histiocytosis (LCH) is a rare disease of unknown etiology that is characterized by the accumulation of CD1a-positive Langerhans-like cells in involved tissues, which are often organized in granulomas [1–4]. LCH may occur in patients of all ages, from neonates to the elderly, with peak incidence occurring in adults between 20 and 40 years of age [3, 4]. While LCH may affect virtually any organ, it most frequently affects the bones, pituitary stalk and skin. Lung involvement is also frequent in adults; it can be present as part

of a multisystem disease or as a single localization of LCH, and it is strongly associated with smoking [5, 6].

The clinical presentation and prognosis of LCH are highly variable. The Histiocyte Society classifies the clinical forms of LCH according to the number and type of organs involved [7]. Single-system LCH affects only one organ/system, particularly bone (unifocal or multifocal) and the lungs in adults [3–6]. Multisystem LCH involves two or more organs/systems, with some localizations, known as "risk organs," i.e., the hematopoietic system, spleen, liver and central nervous system, bearing less favorable prognoses [3, 4]. Thus, the accurate staging of LCH is an important step in managing these patients. Therefore, at diagnosis, a comprehensive clinical evaluation, several laboratory tests and bone imaging are recommended for all adult LCH patients, regardless of the primary manifestation of the disease [8]. A skeletal X-ray survey (including a dental panoramic radiograph) and standard chest X-rays are systematically performed, followed by chest high-resolution computed tomography (HRCT) in case of lung involvement [8]. Bone CT is recommended for specific LCH localizations, such as lesions in the mastoid or vertebrae [8]. Bone magnetic resonance imaging (MRI) may be useful for better assessing contiguous extensions into soft tissues [8]. Additional investigations are performed as needed according to clinical symptoms and signs suggesting specific LCH localizations, such as head MRI in the presence of diabetes insipidus [8].

The investigations that are serially performed during spontaneous or post-treatment patient follow-up examinations vary according to the initial localizations and the eventual occurrence of new symptoms or signs of LCH. Assessing the outcome of LCH in bone using standard imaging techniques remains difficult, because osteolytic lesions require months to heal [9]. ^{18}F-fluorodeoxyglucose positron emission tomography-computed tomography (^{18}F-FDG PET-CT), which combines an anatomical evaluation (CT) with an assessment of the metabolic activity (^{18}F-FDG uptake) of bone lesions, should be particularly useful in this context [10]. Phillips et al. evaluated the usefulness of ^{18}F-FDG PET-CT in children with LCH and bone involvement, and found that PET-CT could identify more bone lesions than standard imaging techniques. This approach also allowed the detection of early responses to treatment [11].

The use of PET-CT in adult LCH patients has been reported in individual or small numbers of cases, and the PET-CT results were not systematically compared with the standard imaging findings [12–14]. The usefulness of PET-CT for managing pulmonary LCH, which affects a substantial proportion of adult patients, remains questionable. Krajiceck et al. reported on PET-CT findings at a given time in a series of adult patients with pulmonary LCH [15]. Nodular lesions displayed significant ^{18}F-FDG uptake, whereas this was rarely the case for cystic lung lesions. This is an important drawback, because the impairment of lung function has been shown to be correlated with the extent of cystic lung lesions found by HRCT [16, 17].

To address these issues, we retrospectively analyzed a series of consecutive patients with systemic LCH (most of them with lung involvement) who were assessed by both standard and PET-CT evaluations at the time the disease was initially staged and during follow-up.

Methods

Study design and subject selection

This retrospective study was conducted by the French National Reference Center for LCH. In this center, ^{18}F-FDG PET-CT has been systematically included as part of the evaluation of adult patients with multisystem LCH since April 2009. All consecutive patients 18 years of age or older with multisystem LCH referred from April 2009 to May 2014 were eligible for this study, provided that they had a PET-CT scan within 8 weeks of their standard evaluation. The diagnosis of LCH was either histologically confirmed by a biopsy of an involved site showing the accumulation of CD1a-positive cells, or based on a typical lung HRCT pattern associated with lytic bone lesions and/or diabetes insipidus and the exclusion of alternative diagnoses [6].

The study was performed in accordance with the tenets of the Declaration of Helsinki and was approved by the institutional review board (CPP Ile de France IV, IRB number 00003835). All patients provided written informed consent for the use of their medical reports for research.

Standard evaluation

The standard patient assessment included a comprehensive clinical evaluation with a thorough history of LCH manifestations, blood laboratory tests, a skeletal X-ray survey, chest X-rays and bone CT and/or MRI scans for specific areas, as recommended [8]. In the case of lung involvement, chest HRCT and lung function tests were performed [6]. For patients with hypothalamic/pituitary manifestations, a head MRI scan and a comprehensive endocrinological evaluation were performed.

The skeletal X-ray survey consisted of anteroposterior and lateral views of the skull and spine, as well as anteroposterior views of the ribs, pelvis, and upper and lower limbs. A dental panoramic radiograph was also obtained. Bone CT examinations comprised multiplanar reconstructions with a bone filter and a millimetric section thickness. MRI studies included short tau inversion recovery (STIR), T2-weighted and T1-weighted (with and without gadolinium injection) images in two orthogonal planes. Lung CT scans were performed with

patients in the supine position during end-inspiratory breath-hold, and were obtained with a reconstructed section thickness of 1 mm or less and a high-spatial frequency algorithm. The images were displayed with a lung window setting (window level: −600 HU; window width 1600 HU). Semi-quantitative nodular and cystic scores were used to assess the extent of lung lesions, as previously described [17]. Chest CT images were also systematically analyzed with a bone window setting (width: 2000; level: 300) to search for eventual LCH involvement in the thoracic bones.

Lung volumes were evaluated by plethysmography, and forced expiratory volume in 1 s (FEV_1) and forced vital capacity (FVC) were determined by the flow curve volume. The diffusing capacity of the lung for carbon monoxide (DL_{CO}) was measured using the single-breath method. Predictive values were determined according to the European Respiratory Society criteria [18]. Obstruction was defined as a ratio of FEV_1 to FVC <70 % [19].

Additional investigations were performed as needed for specific LCH localizations.

^{18}F-FDG PET-CT

Patients fasted for at least 6 h before undergoing whole-body PET-CT, and blood sugar levels were checked to ensure that glycemia was in the normal range. Images were acquired 60 min after an intravenous injection of 5 MBq/kg of ^{18}F-FDG (not exceeding 500 MBq) using a Gemini GXL instrument (germanium oxyorthosilicate-based PET + 16-slice CT; Philips). CT data were acquired without contrast enhancement using the following parameters: 120 kV; 100 mAs; pitch 0.94; slice thickness 2.5 mm. PET data were collected in a 3-dimensional mode, with 2 min per-table-position, and were reconstructed with a line-of-response row-action maximum-likelihood algorithm (LOR-RAMLA).

Visual analysis was performed, and maximum standardized uptake value (SUVmax) was measured for each pathological uptake shown on the manufacturer's review workstation (PETView, Philips Medical Systems). For patients with serial PET-CT scans, a variation of 50 % or greater in the SUVmax of the lesion was considered significant [11].

Data collection

Data on patient demographics, clinical symptoms and signs, and treatments of interest at diagnosis, at the time of each PET-CT scan, and at the last time of follow-up were retrieved from the medical records. Both the standard bone imaging (i.e., skeletal X-ray survey, bone CT and/or MRI) and lung CT scans were interpreted by an expert radiologist (C de MM). All PET-CT scans were analyzed by two experienced nuclear medicine physicians (LV and AV), who had no knowledge of the related clinical history or standard imaging findings.

Evaluation of disease state and response to treatment

The disease state was assessed based on standard evaluations as defined by Histiocyte Society criteria [20]. In brief, if all signs and symptoms were resolved, patients were considered as having non-active disease (NAD). Otherwise, they were classified as having active disease (AD). AD was further subdivided into regressive (improvement of symptoms or signs, no new lesions), stable (persistence of symptoms or signs, no new lesions) or progressive (progression of symptoms or signs and/or appearance of new lesions) disease. LCH response to treatment was classified as better (complete resolution or regression), intermediate (stable or mixed, i.e., new lesions in one site, regression in another site) or worse (progression) [20]. Because specific LCH treatments have virtually no influence on pituitary involvement, this localization was not considered in LCH staging unless new endocrine dysfunction occurred (progressive disease) [8].

The outcome of pulmonary LCH involvement was based on the results of serial lung function tests [17]. The overall lung function outcome was defined by whether there was an increase or decrease of ≥10 % in the FEV_1 and/or FVC, and/or of ≥15 % in the DL_{CO}. In cases of discrepancies, the impaired parameter was used as the overall lung function outcome. If the changes were <10 % for FEV_1 and FVC and <15 % for the DL_{CO}, lung function was considered to be stable. Additionally, the occurrence of a new pneumothorax during follow-up was considered a sign of pulmonary LCH progression [17].

In all cases, disease state and disease response to treatment were assessed without knowledge of the PET-CT results.

Statistical analysis

Descriptive statistics are shown as the mean ± standard deviation or the median (interquartile range [IQR]). The mean SUV variation over time was compared across treatment groups using the nonparametric Mann–Whitney test. The treatment response (defined by a variation of at least 50 % in mean SUVmax) was compared across the treatment groups using Fisher's exact test. All tests were two-sided, and p values of 0.05 or less denoted statistical significance.

Analysis was performed using R 3.2.2 (https://www.R-project.org/) software.

Results

Study population

The medical records of 15 patients with multisystem LCH were reviewed. One patient was excluded because the interval between the standard bone imaging and ^{18}F-FDG PET-CT

scans was greater than 8 weeks. Fourteen patients (37 ± 13 years, 7 men) were included in the study. The diagnosis of LCH was histologically confirmed in 12 patients (bone $n = 6$, lung $n = 4$, skin $n = 1$, peripheral lymph node $n = 1$, cecum $n = 1$; one patient had two-site biopsies). The remaining two patients had a typical lung HRCT pattern with multifocal lytic bone lesions; one of these two patients also had diabetes insipidus.

The initial PET-CT scan was performed at the time of diagnosis of LCH for five patients and at the time of disease reactivation for the remaining nine patients. At this time, all patients had AD, and none were receiving specific treatments for LCH, except substitutive hormonal therapy in the case of pituitary stalk involvement. The clinical manifestations and staging of LCH based on the standard evaluation for each patient are shown in Table 1. In summary, the involved organs were as follows: bone ($n = 13$; unifocal $n = 3$, multifocal $n = 10$), lung ($n = 12$), pituitary stalk ($n = 9$), skin ($n = 3$), mucosa ($n = 4$; genital $n = 2$, oral $n = 2$), lymph node ($n = 1$), soft tissue ($n = 1$), and cecum ($n = 1$). Among the 12 patients with pulmonary LCH involvement, six were current smokers, five were ex-smokers and one was a non-smoker.

^{18}F-FDG PET-CT findings

The initial PET-CT results for each patient are detailed in Table 1. In all but one patient, PET-CT showed hypermetabolic lesions, with a median SUVmax of 5.9 (IQR [4.1–8.7]). PET-CT identified every LCH bone lesion visualized by standard imaging. Bone lesions were hypermetabolic in 11/13 patients. In five patients, PET-CT showed additional hypermetabolic osteolytic lesions. Thyroid ^{18}F-FDG uptake was observed in three patients; this uptake was missed by the standard evaluation in two patients (Table 1 and Figs. 1 and 2). Thyroid ^{18}F-FDG uptake was homogeneous for two patients and was localized to the right thyroid lobe for the third patient. Further evaluation demonstrated specific thyroid LCH localization in two patients, one of whom had associated papillary carcinoma; the other patient was diagnosed with Hashimoto thyroiditis.

None of the nine patients with diabetes insipidus and/or anterior pituitary dysfunction had significant pituitary stalk ^{18}F-FDG uptake, despite abnormal MRI scans in all but one patient (pituitary stalk thickening and/or absence of posterior pituitary bright spot). Because of the initial suspicion of metastatic cancer, patient #4 had a systematic colonoscopy that showed a mild LCH infiltration of the cecum, which was not visualized by PET-CT.

Serial ^{18}F-FDG PET-CT findings

Ten patients had one ($n = 6$) or two ($n = 4$) serial PET-CT scans during their follow-up (Tables 2 and 3). Serial PET-CT scans were performed in six patients after the systemic treatment of LCH (i.e., prednisone and vinblastine and/or cladribine; Table 2). In five of these patients, the serial PET-CT findings after treatment were consistent with the category of disease response (i.e., better, intermediate or worse), based on the standard evaluation and as assessed blinded to the PET-CT results (Table 2, Fig. 3). The remaining patient (#9) was classified as having stable AD after first-line treatment, whereas PET-CT evaluation identified new hypermetabolic osteolytic lesions of both clavicles, denoting disease progression (Table 2).

The serial PET-CT scan results of four untreated patients during the follow-up period were also available. Patients #5 and #14 had refused chemotherapy, patient #8 had inactive multifocal bone disease with new-onset diabetes insipidus, and patient #11 had pulmonary involvement with recurrent pneumothoraces that precluded the use of cladribine because of a disproportionate risk for pleuropulmonary infection complications. As shown in Table 3, the serial PET-CT scan results were in agreement with those of the disease state assessment that was blinded to the PET-CT findings. Patient #11 was classified as AD progressive because of recurrent pneumothoraces during the follow-up period, for which PET-CT assessment does not provide additional information.

Overall, the median (IQR) value of SUV variation over time was −136 % (−484; −95) after cladribine, versus −11 % (−18; +9) after prednisone and vinblastine, and −42 % (−63; −21) in untreated patients ($p = 0.01$, by the Kruskal-Wallis test). When considering the variations in SUVmax ≥50 %, all six patients treated with cladribine improved, none of the three patients who received prednisone and vinblastine improved, and two of the four untreated patients also improved ($p = 0.016$, by Fisher's exact test).

^{18}F-FDG PET-CT assessment of bone LCH

In the 13 patients with bone LCH involvement visualized by standard imaging, PET-CT identified osteolytic lesions in all cases. LCH lesions involved the ribs ($n = 5$), vertebrae ($n = 6$), skull (including the mastoid and maxillae/mandibulae; $n = 19$), pelvis ($n = 20$), long bones ($n = 5$), sternum ($n = 1$) and scapula ($n = 1$). Among these 57 bone lesions, which varied in size from 7 to 47 mm, 41 displayed ^{18}F-FDG uptake (median SUVmax = 5.4, IQR [4.5–7.5]), even for lesions <10 mm in size. At the time of the initial LCH evaluation, PET-CT identified 12 additional lytic bone lesions of the pelvis (patients #1, #11 and #14), the ribs (patient #14), the vertebrae (patient #11) and the jaw (patients #3 and #5), which were missed by the standard evaluation (Table 1).

Serial PET-CT scans were most informative for the evaluation of bone lesions during patient follow-up. The ^{18}F-FDG uptake of bone lesions (SUVmax values)

Table 1 ^{18}F-FDG PET-CT findings of the 14 patients with multisystem LCH compared to those of the standard evaluation[a]

Patient	Sex/age (years)	Standard evaluation findings[a]	^{18}F-FDG PET-CT (SUVmax) results
1	M/19	Bilateral swelling of cervical lymph nodes Mediastinal lymph nodes Lytic lesion of right 6th rib, right humerus, left scapula (MFB) Scattered, thin-walled lung cysts	Bilateral cervical (15), mediastinal (10.3) lymph nodes Lytic lesion of right 6th rib (5.9), bilateral iliac bones (4.5), right sacrum (6.7) Non-hypermetabolic lytic lesions of L5, right humerus, left scapula (MFB)
2	F/53	Dyspnea, skin lesions of the scalp, vulvar ulcerations, tooth mobility Lytic lesion of left maxilla (UFB) Diffuse, thick- and thin-walled lung cysts Treated DI and APD	Lytic lesion of left maxilla (3.4) (UFB)
3	M/56	Dyspnea, tooth mobility Lytic lesion of right mandible (UFB) Diffuse, thick- and thin-walled lung cysts, few nodules Treated DI and APD	Lytic lesions of both mandibles (5.2) and maxillae (6.6) (MFB) ^{18}F-FDG uptake in the right thyroid lobe (3.8)
4	F/49	Right hip pain, dyspnea, cough Lytic lesion of right iliac bone (UFB) Diffuse lung nodules and few thin-walled cysts Thyroid nodules Mild infiltration of cecum[b]	Lytic lesion of right iliac bone (12.8) (UFB) ^{18}F-FDG uptake in lung nodules (2.8) Diffuse ^{18}F-FDG uptake in the thyroid (8.1)
5	M/35	Bilateral parietal swelling, lumbar pain Lytic lesion of both parietal bones, right femur, L3 and right 10th rib (MFB) Scattered, thick-walled lung cysts and nodules	Lytic lesions of both parietal bones (7.8), right femur (4.8), L3 (4.8), right 10th rib (5.9), right mandible (7.4) (MFB)
6	F/31	Dyspnea, left thoracic pain, dizziness, left hearing loss Lytic lesion of left 9th rib, lytic lesion and opacification of left mastoid air cells (MFB) Sequelae of curettage of left mandible lytic lesions Diffuse, thick- and thin-walled lung cysts Treated DI	Lytic lesion of left 9th rib (5.4), left mastoid (11) (MFB)
7	F/52	Dyspnea, cough, diffuse skin lesions, vulvar lesions Diffuse, thick- and thin-walled lung cysts, left pleural thickness (talc pleurodesis) Treated DI and APD	^{18}F-FDG uptake in the skin (median 4), genital mucosa (11.1) ^{18}F-FDG uptake in the left pleura (4.6)[c] Homogeneous ^{18}F-FDG uptake of the thyroid (5.3)
8	M/33	Polyuria/polydipsia, new-onset DI Lytic lesions of both iliac and both femur bones (MFB)	Non-hypermetabolic lytic lesions of both iliac, and both femur bones
9	F/30	Diffuse skin lesions, multifocal soft tissues infiltration, complete tooth loss Lytic lesions of sternum, T8, T9, left iliac and pubic bones (MFB) Sequelae of previous maxillae and mandibles lesions	Multifocal ^{18}F-FDG uptake in soft tissues (median 8.8) Lytic lesion in sternum (4.5), left iliac (3.1) and pubic bones (3.3) (MFB) Non-hypermetabolic lytic lesions of T8, T9
10	M/36	Dyspnea, recurrent bilateral pneumothoraces Lytic lesion of left parietal bone, internal fixation of right femur (MFB) Diffuse thick-walled lung cysts, partial right pneumothorax, bilateral pleural thickness (talc pleurodesis) Treated DI and APD	Non-hypermetabolic lytic lesions of left parietal bone, left iliac bone, ischium and acetabulum, internal fixation of right femur ^{18}F-FDG uptake in the right (10.2) and left (11.3) pleura[c]
11	M/18	Dyspnea, recurrent pneumothoraces, occipital bone defect, pelvic pain	Occipital lytic lesion (SUVmax could not be measured)

Table 1 (continued)

Patient	Sex/age (years)	Standard evaluation findings[a]	^{18}F-FDG PET-CT (SUVmax) results
		Lytic lesions of occipital bone, right trochanter, left acetabulum and left mandible (MFB) Diffuse, thick-walled lung cysts, few nodules, partial bilateral pneumothorax	Lytic lesions of right trochanter (5.4), left acetabulum (4.3), left mandible (4.8), L2 (4.6), left iliac bone (3.4 and 6.2), sacrum (6.2) (MFB)
12	M/25	Dyspnea, cranial vault pain, left temporal, parietal and frontal defect, tooth mobility, gingivitis Lytic lesions of temporal, parietal and frontal left bones with sclerosis (previous surgery), lytic lesion of right mandible (MFB) Diffuse, thick-walled lung cysts Treated DI and APD	Non-hyper metabolic lytic lesions of left temporal, parietal and frontal bones Lytic lesion of right mandible (8.8) ^{18}F-FDG uptake in thick-walled lung cysts (3.4)
13	F/50	Tooth mobility Lytic lesions of left mandible and right maxilla (MFB) Diffuse, thin-walled lung cysts Treated DI	Lytic lesion of left mandible (5), right maxilla (4.2) (MFB)
14	F/28	Dyspnea, cough, cervical, left hip and right thoracic pain, tooth mobility, gingivitis Lytic lesions of C5, right 5th rib, left iliac bone, left ischium, right iliac bone and right mandible (MFB) Diffuse, thick- and thin-walled lung cysts, few nodules Treated DI and APD	Lytic lesions of C5 (6), right 5th rib (4.8), right 3rd rib (8.7), left iliac bone (7.7 and 7.6), left ischium (1.5), right iliac bone (3), right sacrum (15.2), right mandible (9.3) (MFB) ^{18}F-FDG uptake in lung nodules (2.1)

Abbreviations: *LCH* Langerhans cell histiocytosis, *SUVmax* maximum standardized uptake value, *HRCT* high-resolution computed tomography, *L* lumbar vertebra, *C* cervical vertebra, *T* thoracic vertebra, *DI* diabetes insipidus, *APD* anterior pituitary dysfunction, *UFB* unifocal bone, *MFB* multifocal bone

[a] Standard evaluation: comprehensive clinical evaluation, blood laboratory tests, skeletal X-ray survey and lung HRCT for lung involvement. In the case of vertebral or mastoid involvement, bone CT and/or MRI scans were also performed. Only symptoms present at the time of evaluation are indicated

[b] A colonoscopy was performed as part of the diagnostic investigation due to an initial suspicion of metastatic cancer

[c] The ^{18}F-FDG uptake in the pleura was related to previous talc pleurodesis performed for pneumothorax and not to LCH involvement

generally evolved concordantly with disease state, as assessed by the standard evaluation (Tables 2 and 3). Notably, for patients whose bone disease improved, the SUVmax of the bone lesions resolved or decreased by ≥50 % despite the persistence of osteolytic lesions on the concomitant CT scans (Fig. 3). Conversely, for patients whose bone disease was stable or progressive, the SUVmax of the bone lesions remained stable or increased, or new hypermetabolic osteolytic lesions were identified (Tables 2 and 3).

^{18}F-FDG PET-CT findings in pulmonary LCH involvement

Twelve patients of the present series had pulmonary LCH involvement. Lung HRCT scans showed a nodulocystic pattern in six cases (4 with a low nodular and 2 with high nodular score) and an isolated cystic pattern in the remaining six patients. The lung HRCT cystic scores of the 12 patients were as follows: low ($n = 3$), moderate ($n = 1$), high ($n = 4$) and very high ($n = 4$).

As shown in Table 1, only three patients had ^{18}F-FDG uptake in the lungs with low SUVmax values. Patients #4 and #14 (both with a high nodular score) had moderate ^{18}F-FDG uptake in the lung nodules. Among patients with a cystic pattern on the lung HRCT scan, only one patient (#12) had moderate ^{18}F-FDG uptake in thick-walled lung cysts (Fig. 4).

The presence of ^{18}F-FDG uptake in the lungs was not predictive of the response to treatment for pulmonary LCH (Table 4). Notably, patients #6 and #7 had no lung ^{18}F-FDG uptake, and nevertheless experienced significant improvement in lung function after treatment with cladribine (Table 4 and Fig. 5).

Finally, it should be stressed that the ^{18}F-FDG uptake in the pleura observed in patients #7 and #10 did not reflect specific LCH involvement, but instead reflected the inflammatory pleural reaction induced by previous talc pleurodesis performed 42 and 3 months before the PET-CT evaluation, respectively.

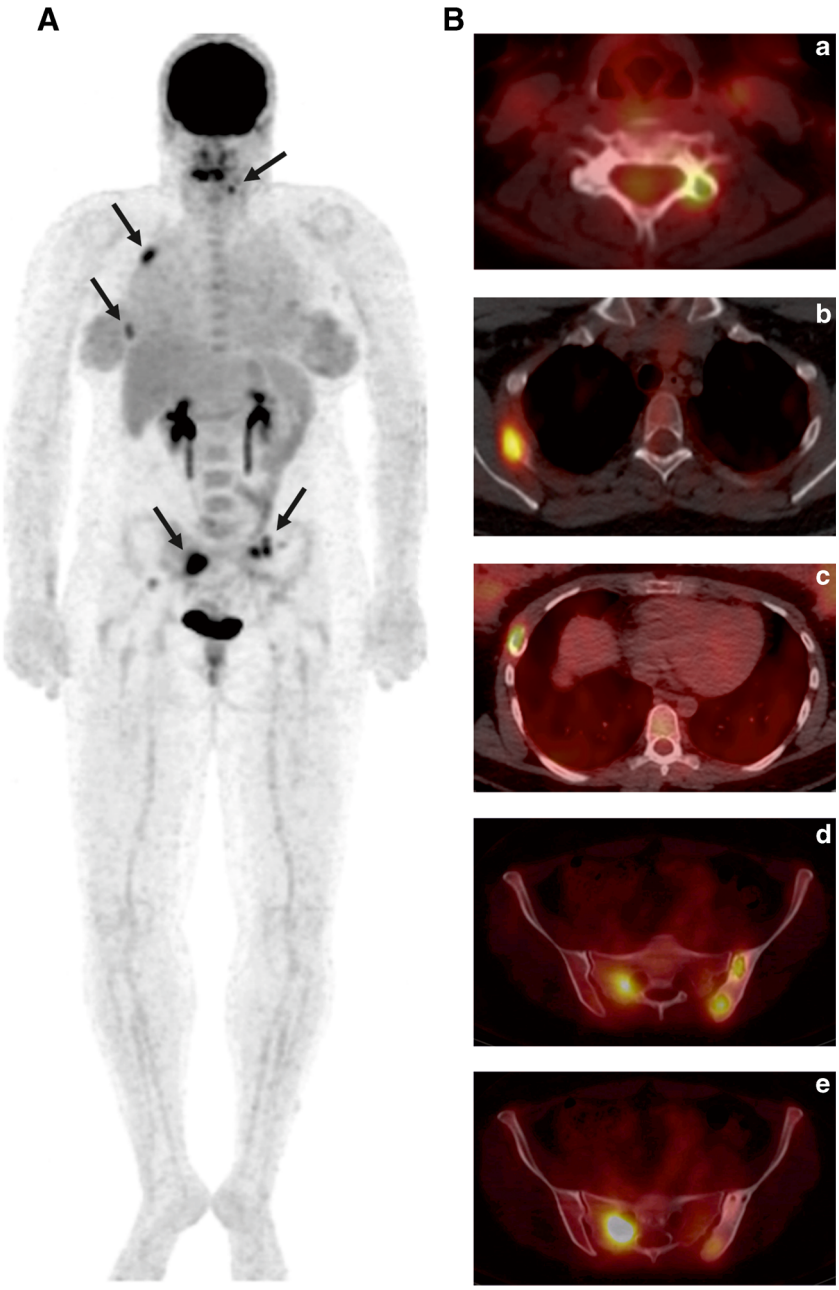

Fig. 1 Patient #14. **A** PET-CT: maximum-intensity projection. **B** PET-CT fused images showing the hypermetabolism of lytic lesions, consistent with active disease: *a* left transverse process of C5; *b* right third rib; *c* right fifth rib; *d* left iliac bone; *e* right sacrum

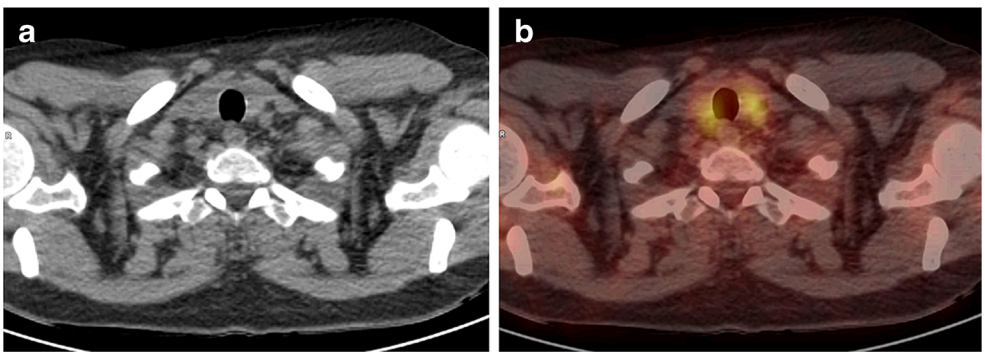

Fig. 2 Patient #7. **a** Thoracic CT at the mediastinal window showing morphologically normal thyroid. **b** Fused PET-CT image showing diffuse, homogeneous thyroid FDG uptake

Table 2 Serial PET-CT findings in treated LCH patients

Patient	PET-CT no. 1[a] (SUVmax)	Treatment	Response to treatment[b]	PET-CT no. 2 (SUVmax)	Treatment	Response to treatment	PET-CT no. 3 (SUVmax)
1	Bilateral cervical (15), mediastinal (10.3) lymph nodes, right 6th rib (5.9), bilateral iliac bones (4.5), right sacrum (6.7)	Prednisone Vinblastine	M+3 AD, worse (left 7th rib) Minimal lung involvement	Bilateral cervical (11.6), mediastinal (8.9) lymph nodes, right 6th rib (4.1), bilateral iliac bones (3.1), right sacrum (7.1), left 7th rib lesion (12.8)	Cladribine	M+6 NAD Minimal lung involvement	No hypermetabolic lesions
3	Both mandibles (5.2) and maxillae (6.6), right thyroid lobe (3.8)	Teeth extraction and curettage	M+9 AD, worse (skin, right mastoid) Stable lung involvement	Left mandible (5.8), left maxillae (6.3), right mastoid lesion (4.4)	Cladribine	M+6 AD, better Stable lung involvement	No hypermetabolic lesions
6	Left 9th rib (5.4), left mastoid (11)	Cladribine	M+6 AD, better Improved lung involvement	No hypermetabolic lesions	NA	NA	NA
7	Skin (median 4), genital mucosa (11.1), thyroid (5.3)	Thyroidectomy and radioactive iodine treatment (papillary carcinoma) Prednisone Vinblastine	M+7 AD, intermediate (stable) Stable lung involvement	Skin (median 6.3), genital mucosa (10.9)	Cladribine	M+7 AD, better Improved lung involvement	Skin (median 2.3), genital mucosa (8.3)
9	Multifocal ^{18}F-FDG uptake in soft tissues (median 8.8), sternum (4.5), left iliac (3.1) and pubic bones (3.3)	Prednisone Vinblastine	M+6 AD, intermediate (stable)	Multifocal ^{18}F-FDG uptake in soft tissues (median 8.1), sternum (4.7), left iliac bone (3.1), and pubic bones (3.1), both clavicles (3.5)	Cladribine	M+15 AD, better	No hypermetabolic lesions
12	Right mandible (8.8), thick-walled lung cysts (3.4)	Teeth extraction and curettage Cladribine	M+5 AD, better Improved lung involvement	No hypermetabolic lesions	NA	NA	NA

Abbreviations: *M+* months after treatment, *LCH* Langerhans cell histiocytosis, *SUVmax* maximum standardized uptake value, *AD* active disease, *NAD* non-active disease, *NA* not applicable

[a] The numbering of patients is the same as that in Table 1. Non-hypermetabolic lesions are not indicated

[b] Disease state was assessed blinded to the PET-CT results and graded according to the Histiocyte Society criteria. For pulmonary involvement, the outcome was classified according to lung function test measurements. Because pituitary involvement is unresponsive to systemic LCH treatment, it was not considered in the assessment of disease activity unless new endocrine dysfunction occurred during the follow-up

Table 3 Serial PET-CT scan findings during the follow-up of patients not specifically treated for LCH

Patient[a] Number	Initial ^{18}F-FDG PET-CT (SUVmax)	Management	Disease state[b] Time interval	Serial ^{18}F-FDG PET-CT (SUVmax)
5	Both parietal bones (7.8), right femur (4.8), L3 (4.8), right 10th rib (5.9), right mandible (7.4)	Refused chemotherapy	AD, regressive Stable lung involvement 5 months	L3 (2.2)
8	Non-hypermetabolic lytic lesions of both iliac bones, left trochanter, neck of right femur	Surveillance	Recurrence AD, progressive 45 months	Lytic lesion of left 6th rib (2.3), right femur (1.9), right iliac bone (6.2), right trochanter (1.6) and left femur (2.2)
11	Occiput (SUVmax unmeasurable), right trochanter (5.4), left acetabulum (4.3), left mandible (4.8), L2 (4.6), left iliac bone (3.4 and 6.2), left sacrum (6.2)	Thoracic surgery for recurrent pneumothoraces	AD, progressive Lung progression 9 months	Occiput (SUVmax unmeasurable), right trochanter (10.2), left acetabulum (3.7), L2 (5.2), left iliac bone (8.6)
14	C5 (6), right 5th rib (4.8), right 3rd rib (8.7), left iliac bone (7.7 and 7.6), left ischium (1.5), right iliac bone (3), right sacrum (15.2), right mandible (9.3), lung nodules (2.1)	Refused chemotherapy Teeth extraction and curettage	AD, regressive Stable lung involvement 5 months	Left iliac bone (2.5 and 7.6), right sacrum (3.4), right mandible (4.9), lung nodules (2.3)

Abbreviations: *LCH* Langerhans cell histiocytosis, *SUVmax* maximum standardized uptake value, *L* lumbar vertebra, *C* cervical vertebra, *AD* active disease

[a] The numbering of patients is the same as that in Table 1

[b] Disease state was assessed by the standard evaluation and graded according to the Histiocyte Society criteria, except in the case with pulmonary involvement, which was based on the occurrence of a new pneumothorax and the results of lung function test measurements. Because pituitary involvement is unresponsive to systemic LCH treatment, it was not considered in the assessment of disease activity unless new endocrine dysfunction occurred during the follow-up

Discussion

In this study evaluating the role of ^{18}F-FDG PET-CT in the management of adult multisystem LCH, we found the following main results: (1) PET-CT identified every LCH localization found by the standard evaluation, with the exception of a mild cecum infiltration, which was incidentally discovered by colonoscopy; (2) in half of the patients, PET-CT showed additional localized ^{18}F-FDG uptake, mostly by osteolytic lesions but also by thyroid abnormalities; (3) during follow-up, PET-CT was very useful for the assessment of the spontaneous outcome and response to treatment of the disease; (4) PET-CT was only slightly helpful for the management of pulmonary involvement.

The assessment of bone LCH remains difficult because of the absence of a gold standard examination. A skeletal X-ray survey is the first investigation recommended, but has poor sensitivity regarding specific localizations such as those in the vertebrae and pelvic bones [8]. Bone CT and MRI scans can provide additional information, but are not systematically performed and are not among the first investigations to be carried out in a given patient [8]. Whole-body MRI scans have been proposed as an alternative for assessing bone LCH involvement in children, but this method does not accurately assess the activity of bone disease [21].

An important advantage of ^{18}F-FDG PET-CT is that it provides both a precise anatomical evaluation (CT) and an assessment of the metabolic activity (^{18}F-FDG uptake) of bone lesions. In the present study, ^{18}F-FDG PET-CT scans were more accurate than the standard evaluation in identifying bone LCH localizations. Importantly, in all cases, these additional bone LCH sites had an osteolytic pattern on the CT scans, which was consistent with LCH involvement. PET-CT scans showed additional lesions in 5/13 (40 %) patients with bone LCH. More precisely, this approach identified 12 additional lesions that mainly concerned not only the pelvis and the jaw but also the ribs and vertebrae. These findings resulted in a change in disease status from unifocal to multifocal bone disease, which has consequences for the management of these patients, who warrant closer follow-up and eventually the initiation of

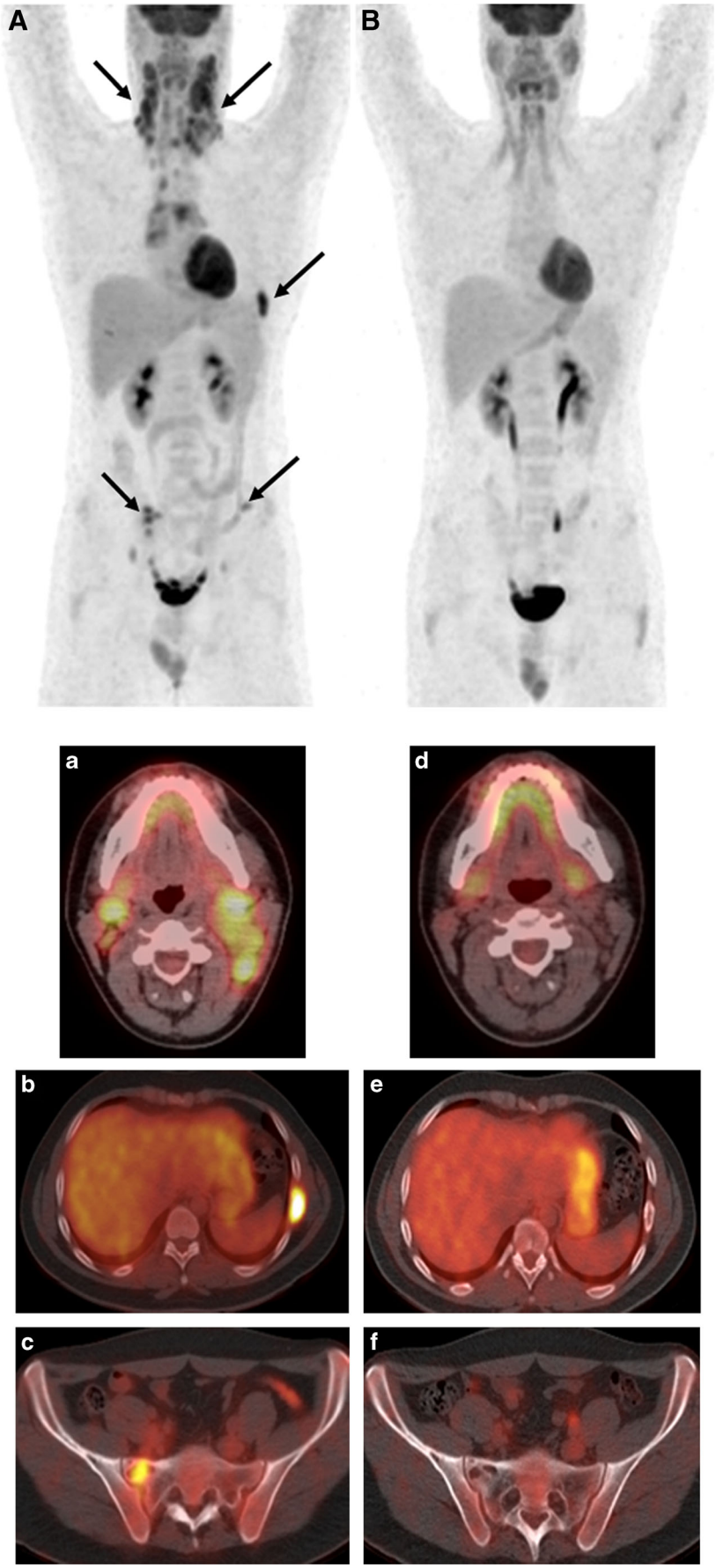
A
B
a
d
b
e
c
f

◀ **Fig. 3** Patient #1. **A** PET: maximum-intensity projection before treatment with cladribine, showing multiple hypermetabolic lesions. PET-CT fused images showing hypermetabolism of *a* bilateral cervical lymph nodes, *b* lytic lesions of the left sixth rib, *c* lytic lesion of the right sacrum. **B** PET: maximum-intensity projection after treatment with cladribine, showing the resolution of all metabolic lesions, *d* regression of the cervical lymph nodes, *e* regression of the hypermetabolism of the left sixth rib with the persistence of a small lytic lesion on CT, *f* regression of the hypermetabolism of the right sacrum with the persistence of a lytic lesion on CT

systemic treatment [8]. Our results are consistent with those of a study conducted by Phillips et al. with a cohort of pediatric LCH patients, in which ^{18}F-FDG PET identified 35 % more lesions than did the standard evaluation [11]. In this study, PET was found to be less sensitive than MRI for spine LCH localizations, but importantly, PET images were not coupled with CT scans at the same time. The absence of concomitant bone CT scans also explains the results of another pediatric study which found ^{18}F-FDG PET to be less sensitive than bone MRI [22]. Furthermore, PET missed very small bone lesions, whose clinical impact is questionable.

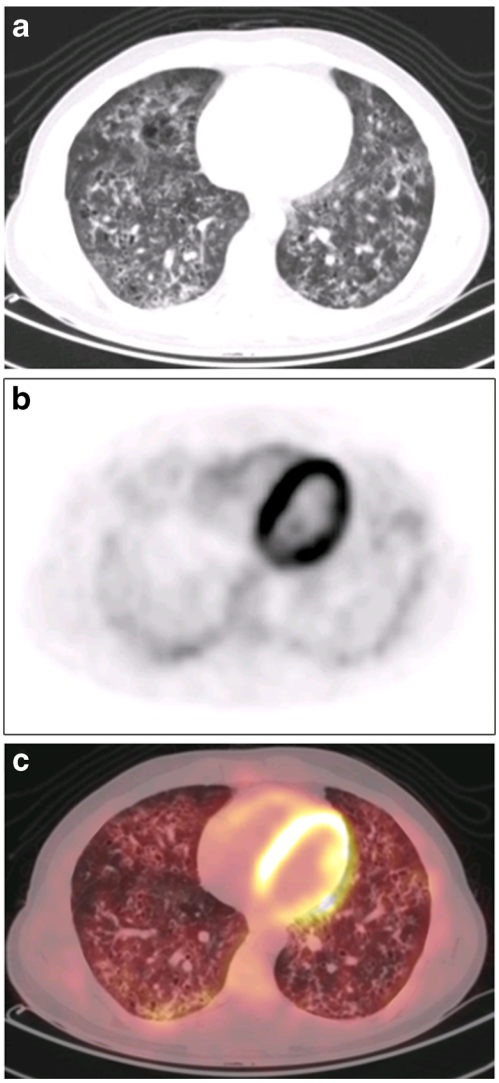

Fig. 4 Patient #12. **a** CT part of PET-CT examination showing thick-walled lung cysts; **b** PET image showing moderate but significant uptake (SUVmax = 3.4) in these cysts; **c** corresponding fused PET-CT image

^{18}F-FDG uptake provided valuable information by differentiating old, inactive lesions from active lesions. Indeed, bone lesion sclerosis, which is indicative of bone lesion healing, may take months to occur [9]. Furthermore, significant variations (≥50 % of SUVmax) in the intensity of bone ^{18}F-FDG uptake were correlated with disease state or response to treatment during follow-up, based on the standard evaluation. Thus, a decrease in SUVmax was associated with a favorable LCH outcome, despite the persistence of bone lysis on bone CT scans. Conversely, an increase in or the appearance of bone ^{18}F-FDG uptake during follow-up was indicative of LCH progression. This finding is in agreement with Phillips's study of pediatric LCH, as well as with preliminary reports of adult LCH [11, 13, 14, 22, 23]. The strength of our study is that the PET-CT findings were uniformly and blindly compared with those of the recommended, standard patient evaluation.

Another salient finding of our study was the identification by PET-CT of thyroid ^{18}F-FDG uptake in three of 14 patients, which is more frequent than previously reported in LCH [24–26]. In two of these three patients, this ^{18}F-FDG uptake was related to thyroid LCH involvement, whereas it was secondary to Hashimoto thyroiditis in the third patient. Most importantly, in one patient, thyroid LCH involvement was associated with papillary carcinoma. Thus, histological confirmation should be obtained in the case of thyroid ^{18}F-FDG uptake in patients with LCH [27].

Other LCH localizations were also identified by PET-CT in this study, including lesions in the lymph nodes, soft tissues and genitals. In the case of lymph node involvement, a tissue biopsy should be promptly considered to rule out alternative diagnoses, particularly lymphoma [28, 29].

A minority of our patients (25 %) with pulmonary LCH involvement shown by lung CT scans displayed moderate ^{18}F-FDG uptake on the PET-CT scans. Two of these three patients had a high nodular lung CT score, and the remaining patient had thick-walled cysts; these findings are consistent with those of a previous report, although the intensity of lung ^{18}F-FDG uptake was lower in our series [15]. Importantly, the presence or absence of lung ^{18}F-FDG uptake was not correlated with disease severity, outcome or response to treatment. Therefore, PET-CT appears to be of little use in the management of LCH with pulmonary involvement. Finally, ^{18}F-FDG uptake in the pleura may be observed in cases with previous talc pleurodesis for pneumothorax.

Interestingly, efficient new PET-CT systems allow the acquisition of additional dedicated (full inspiratory/breath-hold) lung CT scans with quality equivalent to that of standalone CT. Thus, when a PET-CT is performed in a patient with LCH

Table 4 Lung function outcome of treated LCH patients with lung involvement compared to PET-CT findings

Patient	HRCT pattern Nodular/cystic (score)	PFTs[a]	PET-CT no.1 ^{18}F-FDG uptake	Treatment	PFT outcomes[b]	PET-CT no.2 ^{18}F-FDG uptake	Treatment	PFT outcomes	PET-CT no.3 ^{18}F-FDG uptake
1	Thin-walled cysts (0,4)	Normal	No	Prednisone/ vinblastine	Normal	No	Cladribine	Normal	No
3	Thick- and thin-walled cysts (3,22)	FVC 57 % FEV_1 44 % DL_{CO} 40 %	No	No	Stable	No	Cladribine	Stable	No
6	Thick- and thin-walled cysts (6,19)	DL_{CO} 48 %	No	Cladribine	Improved	No	NA	NA	NA
7	Thick- and thin-walled cysts (0,24)	FVC 47 % FEV_1 33 % DL_{CO} 43 %	No	Prednisone/ vinblastine	Deteriorated	No	Cladribine	Improved	No
12	Thick-walled cysts (0,14)	FVC 52 % FEV_1 40 % DL_{CO} 22 %	Yes	Cladribine	Improved	No	No	Stable	No

Abbreviations: *LCH* Langerhans cell histiocytosis, *HRCT* high-resolution computed tomography, *PFTs* pulmonary function tests, *FEV_1* forced expiratory volume in 1 s, *FVC* forced vital capacity, *DL_{CO}* diffusing capacity of the lung for carbon monoxide

[a] Only abnormal PFT parameters are indicated. The results are expressed as the percentage of the predictive value

[b] The overall lung function outcome was defined by whether there was an increase or decrease of ≥10 % in the FEV_1 and/or FVC, and/or of ≥15 % in the DL_{CO}. In cases of discrepancies, the impaired parameter was used as the overall lung function outcome. If the changes were <10 % for FEV_1 and FVC and <15 % for the DL_{CO}, lung function was considered stable

lung involvement, a "one-stop shop" approach, providing the valuable information of both PET-CT and lung HRCT in a single visit, could improve patient convenience.

We did not observe any pituitary stalk ^{18}F-FDG uptake in our patients with diabetes insipidus and/or anterior pituitary dysfunction, despite abnormalities on the MRI scans (pituitary stalk thickening and/or absence of posterior pituitary bright spot). Thus, although PET-CT scans may show ^{18}F-FDG uptake in cases with a hypothalamic and/or pituitary mass [14], pituitary MRI appears to be a more valuable mode of investigation for this LCH localization.

This study has several limitations, which are mainly due to the small sample size and its retrospective design. In particular, serial PET-CT evaluations were not performed at similar time points during patient follow-up. For children treated with vinblastine, disease response to treatment is usually evaluated 6 weeks after the end of the induction phase of weekly injection treatments [11]. In the case of treatment with cladribine, which is administered in monthly cycles, evaluating the response at 3 months of treatment is reasonable. In untreated patients, serial PET-CT scans should be performed on a case-by-case basis, guided by clinical outcome.

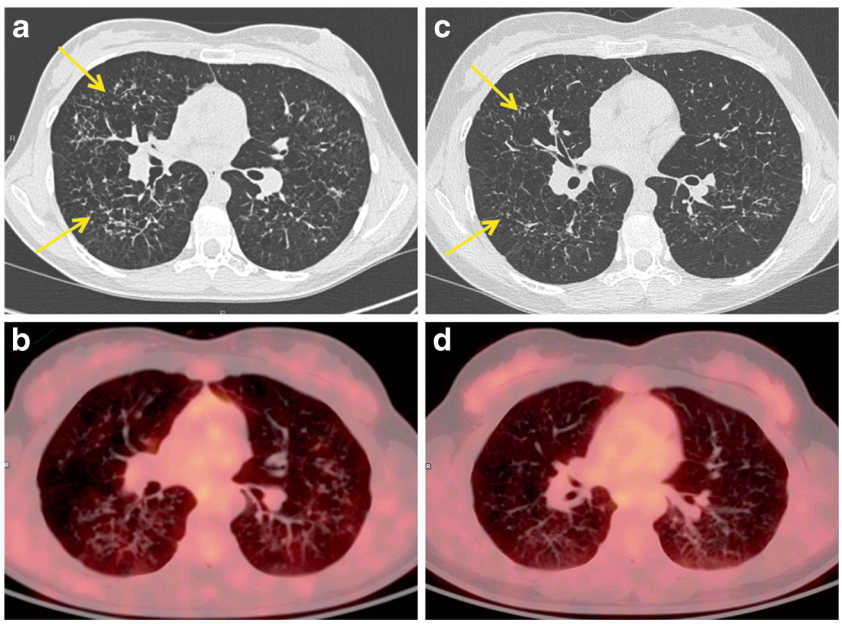

Fig. 5 Patient #6. **a** Lung HRCT before treatment showing diffuse, thick- and thin-walled lung cysts (*arrows*). **b** Fused PET-CT image before treatment with no significant lung uptake. **c** Lung HRCT after treatment with cladribine showing the partial regression of cysts (*arrows*). **d** Fused PET-CT image after treatment showing no significant changes

In summary, with the exception of pulmonary and pituitary involvement, our study strongly suggests that whole-body ^{18}F-FDG PET-CT is a valuable technique for evaluating adult patients with multisystem LCH, and could replace the standard evaluation. Serial PET-CT scans are also very useful for evaluating response to treatment, particularly for cases with bone LCH involvement.

Acknowledgments The authors thank M. Mao (Assistance Publique-Hôpitaux de Paris; Service de Pneumologie, Hôpital Saint-Louis, Paris, France) and E. Savariau (Institut Universitaire d'Hématologie, Service d'Infographie, Hôpital Saint-Louis, Paris, France) for their technical assistance.

Compliance with ethical standards

Funding This study received no funding.

Conflict of interest The authors declare that they have no conflict of interest.

Ethical approval All procedures performed in studies involving human participants were in accordance with the ethical standards of the institutional research committee and with the 1964 Declaration of Helsinki and its later amendments or comparable ethical standards.

Informed consent Informed consent was obtained from all individual participants included in the study.

References

1. Emile JF, Abla O, Fraitag S, Horne A, Haroche J, Donadieu J, et al. Revised classification of histiocytoses and neoplasms of the macrophage-dendritic cell lineages. Blood. 2016;127:2672–81.
2. Picarsic J, Jaffe R. Nosology and pathology of Langerhans cell histiocytosis. Hematol Oncol Clin North Am. 2015;29:799–823.
3. Stockschlaeder M, Sucker C. Adult Langerhans cell histiocytosis. Eur J Haematol. 2006;76:363–8.
4. Weitzman S, Egeler RM. Langerhans cell histiocytosis: update for the pediatrician. Curr Opin Pediatr. 2008;20:23–9.
5. Suri H, Yi ES, Nowakowski GS, Vassallo R. Pulmonary langerhans cell histiocytosis. Orphanet J Rare Dis. 2012;7:16.
6. Tazi A, de Margerie C, Naccache JM, Fry S, Dominique S, Jouneau S, et al. The natural history of adult pulmonary Langerhans cell histiocytosis: a prospective multicentre study. Orphanet J Rare Dis. 2015;10:30.
7. Writing Group of the Histiocyte Society. Histiocytosis syndromes in children. Lancet. 1987;1:208–9.
8. Girschikofsky M, Arico M, Castillo D, Chu A, Doberauer C, Fichter J, et al. Management of adult patients with Langerhans cell histiocytosis: recommendations from an expert panel on behalf of Euro-Histio-Net. Orphanet J Rare Dis. 2013;8:72.
9. Meyer JS, Harty MP, Mahboubi S, Heyman S, Zimmerman RA, Womer RB, et al. Langerhans cell histiocytosis: presentation and evolution of radiologic findings with clinical correlation. Radiographics. 1995;15:1135–46.
10. Kaste SC, Rodriguez-Galindo C, McCarville ME, Shulkin BL. PET-CT in pediatric Langerhans cell histiocytosis. Pediatr Radiol. 2007;37:615–22.
11. Phillips M, Allen C, Gerson P, McClain K. Comparison of FDG-PET scans to conventional radiography and bone scans in management of Langerhans cell histiocytosis. Pediatr Blood Cancer. 2009;52:97–101.
12. Binkovitz LA, Olshefski RS, Adler BH. Coincidence FDG-PET in the evaluation of Langerhans' cell histiocytosis: preliminary findings. Pediatr Radiol. 2003;33:598–602.
13. Blum R, Seymour JF, Hicks RJ. Role of 18FDG-positron emission tomography scanning in the management of histiocytosis. Leuk Lymphoma. 2002;43:2155–7.
14. Lee HJ, Ahn BC, Lee SW, Lee J. The usefulness of F-18 fluorodeoxyglucose positron emission tomography/computed tomography in patients with Langerhans cell histiocytosis. Ann Nucl Med. 2012;26:730–7.
15. Krajicek BJ, Ryu JH, Hartman TE, Lowe VJ, Vassallo R. Abnormal fluorodeoxyglucose PET in pulmonary Langerhans cell histiocytosis. Chest. 2009;135:1542–9.
16. Canuet M, Kessler R, Jeung MY, Metivier AC, Chaouat A, Weitzenblum E. Correlation between high-resolution computed tomography findings and lung function in pulmonary Langerhans cell histiocytosis. Respiration. 2007;74:640–6.
17. Tazi A, Marc K, Dominique S, de Bazelaire C, Crestani B, Chinet T, et al. Serial computed tomography and lung function testing in pulmonary Langerhans' cell histiocytosis. Eur Respir J. 2012;40:905–12.
18. European Respiratory Society. Standardized lung function testing. Eur Respir J Suppl. 1993;16:1–100.
19. Pauwels RA, Buist AS, Calverley PM, Jenkins CR, Hurd SS. Global strategy for the diagnosis, management, and prevention of chronic obstructive pulmonary disease. NHLBI/WHO Global Initiative for Chronic Obstructive Lung Disease (GOLD) workshop summary. Am J Respir Crit Care Med. 2001;163:1256–76.
20. Broadbent V, Gadner H. Current therapy for Langerhans cell histiocytosis. Hematol Oncol Clin North Am. 1998;12:327–38.
21. Goo HW, Yang DH, Ra YS, Song JS, Im HJ, Seo JJ, et al. Whole-body MRI of Langerhans cell histiocytosis: comparison with radiography and bone scintigraphy. Pediatr Radiol. 2006;36:1019–31.
22. Mueller WP, Melzer HI, Schmid I, Coppenrath E, Bartenstein P, Pfluger T. The diagnostic value of 18F-FDG PET and MRI in paediatric histiocytosis. Eur J Nucl Med Mol Imaging. 2013;40:356–63.
23. Adam Z, Szturz P, Vanicek J, Moulis M, Pour L, Krejci M, et al. Cladribine (2-chlorodeoxyadenosine) in frontline chemotherapy for adult Langerhans cell histiocytosis: a single-center study of seven cases. Acta Oncol. 2013;52:994–1001.
24. Cai YF, Wang QX, Ni CJ, Dong SY, Lv L, Li Q, et al. A case report: the diagnosis and therapeutic evaluation for a rare disease of langerhans cell histiocytosis involving thyroid. Medicine (Baltimore). 2015;94:e1891.
25. Giovanella L, Ceriani L, Crippa S, Mazzucchelli L. Imaging in endocrinology: Langherans cell histiocytosis of the thyroid gland detected by 18FDG-PET/CT. J Clin Endocrinol Metab. 2007;92:2866–7.
26. Uchiyama M, Watanabe R, Ito I, Ikeda T. Thyroid involvement in pulmonary Langerhans cell histiocytosis. Intern Med. 2009;48:2047–8.
27. Vergez S, Rouquette I, Ancey M, Serrano E, Caron P. Langerhans cell histiocytosis of the thyroid is a rare entity, but an association with a papillary thyroid carcinoma is often described. Endocr Pathol. 2010;21:274–6.
28. Das DK, Sheikh ZA, Alansary TA, Amir T, Al-Rabiy FN, Junaid TA. A case of Langerhans' cell histiocytosis associated with Hodgkin's lymphoma: fine-needle aspiration cytologic and histopathological features. Diagn Cytopathol. 2016;44:128–32.
29. Naumann R, Beuthien-Baumann B, Fischer R, Kittner T, Bredow J, Kropp J, et al. Simultaneous occurrence of Hodgkin's lymphoma and eosinophilic granuloma: a potential pitfall in positron emission tomography imaging. Clin Lymphoma. 2002;3:121–4.